Photonic crystal cavities in silicon dioxide

Yiyang Gong[a)] and Jelena Vučković

Department of Electrical Engineering, Stanford University, Stanford, California 94305, USA

One dimensional nanobeam photonic crystal cavities fabricated in silicon dioxide are considered in both simulation and experiment. Quality factors of over 10^4 are found via simulation, while quality factors of over 5×10^3 are found in experiment, for cavities with mode volumes of $2.0(\lambda/n)^3$ and in the visible wavelength range 600–716 nm. The dependences of the cavity quality factor and mode volume for different design parameters are also considered. © *2010 American Institute of Physics.* [doi:10.1063/1.3297877]

Silicon complementary metal-oxide-semiconductor compatible materials can be integrated with electronics, and thus can have a large impact in computation, communication, and sensors. One important component of an optical system is a photonic cavity, able to store light and spectrally filter signals. The photonic crystal (PC) cavity is one type of optical cavity that allows for both high quality (Q) factors and low mode volumes (V_{mode}), having ubiquitous use in cavity quantum electrodynamics (cQED),[1] low threshold lasers,[2] and optical control.[3] One of the most developed PC systems is the system of two dimensional (2D) waveguides and cavities in a free-standing membrane, relying on total internal reflection for confinement in the third dimension. Silicon is transparent in the near infrared regime, and is heavily used for telecommunication purposes near the wavelength of 1.5 μm. However, silicon absorbs heavily in the visible wavelength range, and would be difficult to employ in light emitting and waveguiding devices at the visible wavelengths.

Silicon dioxide (SiO$_2$ or silica), on the other hand, is transparent at the visible wavelengths, and similar to silicon, is a promising material due to its low cost, compatibility with electronics and established fabrication techniques. The main hurdle in manufacturing photonic crystals in silica is its low index of refraction ($n=1.46$). However, perturbation cavities that modulate the index of refraction in a waveguide system can be made even in low index materials. This approach has been used in creating high-Q cavities in 2D PCs in both silicon[4–6] and low index materials such as silicon nitride (Si$_3$N$_4$),[7] which has index $n=2.0$, higher than that of SiO$_2$. Whereas a full photonic band gap in a 2D photonic crystal is difficult to achieve in low index materials, one dimensional (1D) nanobeam cavities that employ a gentle confinement technique enable high confinement with a small or incomplete band gap, while relying on total internal reflection in both directions perpendicular to the beam length. Recent developments in 1D nanobeam cavities with "potential well" designs have achieved the same Q-factors in silicon as in 2D photonic crystal cavities with comparable mode volumes,[8,9] while also opening the door for high-Q cavities in Si$_3$N$_4$ for applications of nano-optomechanical coupled resonators[10] and coupling to active materials.[11]

In this letter, we design and fabricate 1D nanobeam cavities in silica. We follow the ladder cavity design used in Si and Si$_3$N$_4$,[10,12] but consider a silica slab suspended in free space, with lattice constant a, width w, slab thickness d, hole width h_x, and hole height h_y, as shown in Fig. 1(b). We first obtain the band diagram of a periodic (or unperturbed) nanobeam waveguide using the three dimensional finite difference time domain (FDTD) method with Bloch boundary conditions. A sample band diagram is shown in Fig. 1(c) for a beam with parameters: lattice constant a, $w=3a$, $d=0.9a$, $h_x=0.5a$, and $h_y=0.7w$, and also for a beam with the same parameters, except with lattice constant $a'=0.9a$. As expected, the structure with the smaller lattice constant has slightly higher band frequencies, as this structure supports modes that have higher overlap with air. Because the lowest band edge mode of the structure with lattice constant a' (mode at the π/a' point) lies in the band gap of the structure with lattice constant a, it can serve as the defect mode in a beam with lattice constant a, which acts as the photonic crystal mirror.
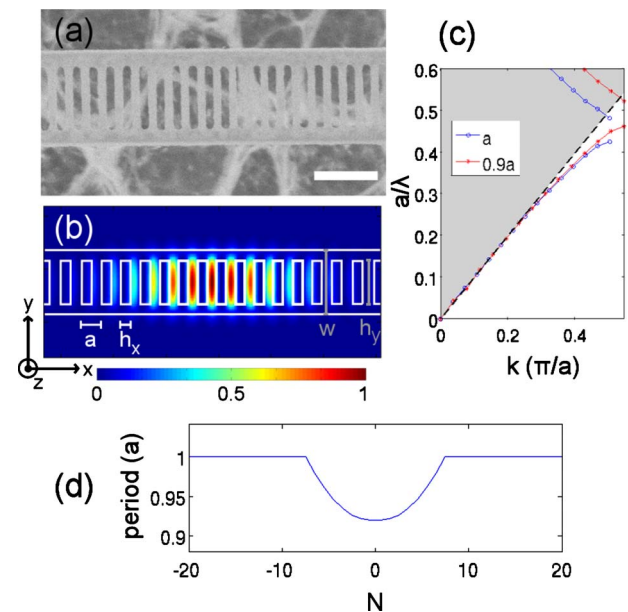

FIG. 1. (Color online) (a) The fabricated 1D nanobeam cavity. Marker denotes 1 μm. (b) The electric field intensity ($|E|^2$) of the fundamental mode supported by the cavity. (c) Band diagram for a beam with lattice constant a, $w=3a$, $d=0.9a$, $h_x=0.5a$, and $h_y=0.7w$, and another beam with the same parameters except for lattice constant $a'=0.9a$. The dashed line indicates the light line in free space. (d) Design of the cavity. The plot shows the period (a) along the length of the beam as a function of N, the layer number counted from the center of the cavity.

a)Electronic mail: yiyangg@stanford.edu.

Next, we use the perturbation design suggested by previous references and introduce a parabolic relationship between the lattice constant and the x-coordinate, thus forming an optical potential well.[13] In particular, we choose a minimum effective lattice constant of $0.90a$ at the center of the potential well, and the remainder of the lattice constants as shown in Fig. 1(d). The perturbations of lattice constants span 7 periods away from the center of the cavity. We simulate the full cavity structure again using the FDTD method, with $a=20$ units and perfectly matched layer absorbing boundary conditions, and obtain the fundamental transverse electric (TE)-like mode with frequency $a/\lambda=0.454$, $Q=1.6 \times 10^4$, $V_{mode}=2.0(\lambda/n)^3$, and electric field intensity ($|E|^2$) shown in Fig. 1(b). This represents a more than one order of magnitude increase in Q-factor and a sevenfold reduction in mode volume compared to a 5 μm diameter silica microdisk cavity with the same silica thickness, again obtained in FDTD simulations. The pure silica microdisks have Q and V_{mode} comparable to similar sized microdisk cavities fabricated in silicon rich oxide, which has slightly higher refractive index ($n=1.7$).[14] While silica microdisks with $Q=10^5$ have been achieved,[15] there remains a tradeoff between the Q and V_{mode}, and silica microdisks with $Q>10,000$ have radii greater than 5 μm and thicknesses greater than 270 nm.

We also simulate the effect of the number of photonic crystal mirror layers on the cavity Q. In particular, we define the quality factor in the direction $\hat{i}$ as $Q_i=\omega U/P_i$, where ω is the frequency of the mode, U is the total energy of the mode, and P_i is the power radiated in the $\hat{i}$ direction, computed by taking the integral of the time averaged Poynting vector across a plane. We separate $Q_{tot}=1/(1/Q_\perp+1/Q_\parallel+1/Q_{PC})$, where Q_{PC} corresponds to radiation leaked through the ends of the silica beam [in the x direction of Fig. 1(b)], $Q_\parallel$ corresponds to radiation leaked out of the beam transverse to the long axis of the beam within the $z=\pm d/2$ plane (in the general y direction), and $Q_\perp$ corresponds to the remaining radiation leaked transverse to the beam long axis (in the general z direction).[13] We plot the dependence of the various Qs as a function of the number of layers of photonic crystal mirrors in Fig. 2(a). We see that the gentle confinement method enables high reflectivity mirrors even in silica, as Q_{PC} continuously increases with the addition of more PC mirror layers. In the case of a 1D nanobeam, Q is limited by loss in the directions where the mode is confined by total internal reflection, namely $Q_\perp$ and $Q_\parallel$. As seen in Fig. 2(a), the limiting factor in Q_{tot} is $Q_\perp$ in this case. Thus, Q_{tot} could be increased by improving the design of the periods that correspond to the photonic crystal cavity, possibly by parameter search, genetic algorithms,[16] or inverse designs.[17,18]

Furthermore, we simulate the cavity with the same pattern of holes in the x-direction, while changing the beam width w and thickness d, keeping $h_x=0.5a$ and $h_y=0.7w$. The resulting limiting Q (the parallel sum of $Q_\perp$ and $Q_\parallel$) and V_{mode} are shown in Figs. 2(b) and 2(c), respectively. We see that both the Q-factor and V_{mode} increase with the slab width and thickness, which is expected as larger cavities have higher confinement but higher mode volumes. In fact, we observe that for small widths and thickness [lower left of Figs. 2(b) and 2(c)], the cavity mode is not as well confined to the center of the beam. In order to employ this cavity in cQED applications, we need to maximize the Q/V_{mode} ratio.
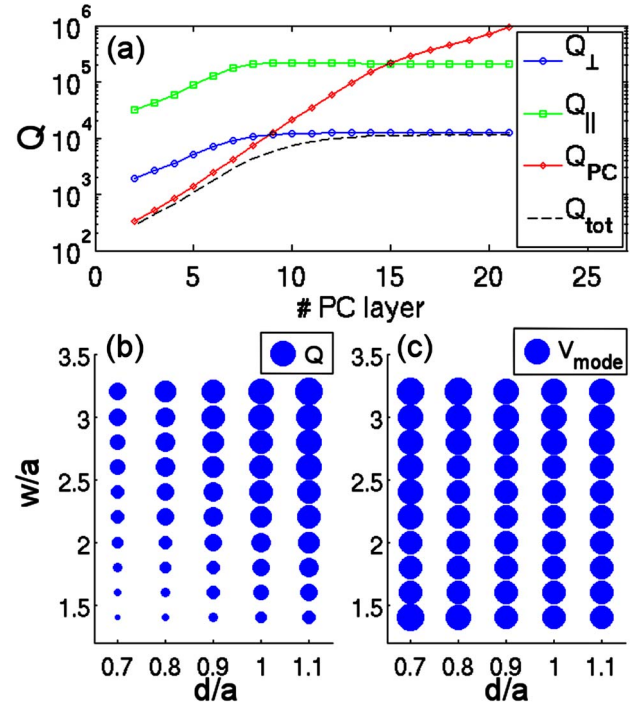

FIG. 2. (Color online) (a) The direction specific Q-factors of the nanobeam cavity as a function of the number of photonic crystal mirror layers surrounding the cavity. With respect to Fig. 1(b), $Q_\perp$ corresponds to radiation leaked in the z direction, $Q_\parallel$ corresponds to radiation leaked in the y direction, and Q_{PC} corresponds to radiation leaked in the x direction. Q_{tot} is the parallel sum of $Q_\perp$, $Q_\parallel$, and Q_{PC}. (b) The Q-factors and (c) the mode volumes of cavities with the same air hole design, but different beam widths and thicknesses. The reference dot sizes are for $Q=2.0\times10^4$ and $V_{mode}=2.0(\lambda/n)^3$ in (b) and (c), respectively.

Such a maximum is achieved with $w=2.6a$ and $d=1.1a$, with $Q=2.0\times10^4$ and $V_{mode}=1.8(\lambda/n)^3$.

We next fabricate the cavity with the same dimensions as above. We start by oxidizing a silicon wafer, forming a 270 nm layer of SiO_2 on top of silicon. Next, e-beam lithography is performed with a 250 nm layer of ZEP-520A as the resist. After development of the resist, the pattern is transferred to the oxide layer with a $CHF_3:O_2$ (100 SCCM/2 SCCM ratio) chemistry dry etch. Finally, the beam is undercut with a 1.0 Torr XeF_2 dry etch, removing approximately 4 μm of silicon under the oxide layer. The final fabricated structure is shown in Fig. 1(a). We vary the lattice constant a in fabrication to create cavities with a variety of wavelengths.

We characterize the cavities using the cross-polarized reflectivity measurement technique.[19,20] In summary, white light linearly polarized 45° from the cavity polarization is directed at the cavity through an objective lens from above (z direction), and emission in the polarization orthogonal to the excitation (135°) is collected also from above and detected by a spectrometer. The fundamental mode of the cavity is linearly polarized in the direction perpendicular to the beam length [y-polarized in Fig. 1(b)], much like the fundamental TE mode of a rectangular slab waveguide. We observe cavities of different resonant wavelengths that span 600–716 nm in the visible wavelength range for different lattice constants, as shown in Fig. 3(a). The cavities are shown from left to right with increasing a. The measured cavity wavelengths and Qs of the cavities are plotted in Fig. 3(b). While the measured $Q=5000$ is lower than the simulated value of 20 000, the reduced value can be attributed to fabrication
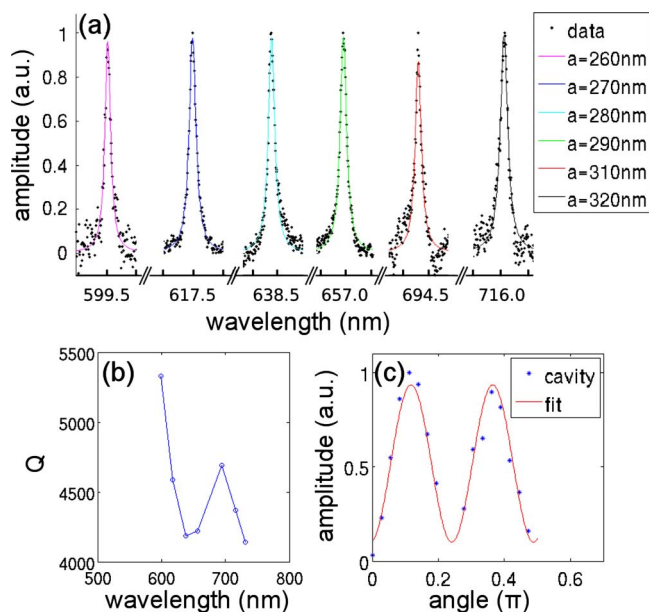
FIG. 3. (Color online) (a) The cavities spectra measured in reflectivity from structures with different lattice constants are normalized and shown together, with fits to Lorentzian lineshapes plotted on top of the data points. The cavity spectra are shown from left to right with increasing a, and wavelength tick marks are spaced with 0.5 nm. (b) The Qs of the cavities shown in part (a) plotted against the wavelengths of the cavities. (c) The angle dependence of the reflectivity amplitude. The horizontal axis corresponds to the half-waveplate angle, which is placed in front of the objective lens that is in front of the chip (and thus placed in both the incident and collection paths). The fit to the reflectivity amplitude shows a period very close to $\pi/4$, indicating a linearly polarized cavity mode.

tolerances of the hole positions and edge roughness of the etched structure. Nevertheless, the experimentally achieved Q is a significant fraction of the simulated value. Similarly, the local variations of Q in Fig. 3(b) can be attribute to the same causes. By placing a half-waveplate in the incident/collection path, we confirm that the observed cavity mode is linearly polarized, as the angle dependent reflectivity amplitude has a period of $\pi/4$ with respect to the half-waveplate angle [Fig. 3(c)].

In conclusion, we have demonstrated a photonic crystal cavity in silica with theoretical Q-factors above 10^4, and experimental Q-factors above 5×10^3, while maintaining low mode volumes of $2.0(\lambda/n)^3$. Such a system could be enhanced by improving the cavity design for higher Q-factors through manipulation of the cavity hole placement. In addition, the coupling of emitters, such as silicon nanocrystals embedded in silica[21] or organic molecules deposited on the cavity surface,[22] to this low index system could be explored. Finally, the silica cavity could be employed to couple optical fields and mechanical oscillations.

[1] D. Englund, D. Fattal, E. Waks, G. Solomon, B. Zhang, T. Nakaoka, Y. Arakawa, Y. Yamamoto, and J. Vučković, Phys. Rev. Lett. **95**, 013904 (2005).
[2] H. Altug, D. Englund, and J. Vučković, Nat. Phys. **2**, 484 (2006).
[3] I. Fushman, E. Waks, D. Englund, N. Stoltz, P. Petroff, and J. Vučković, Appl. Phys. Lett. **90**, 091118 (2007).
[4] M. Notomi, T. Tanabe, A. Shinya, E. Kuramochi, H. Taniyama, S. Mitsugi, and M. Morita, Opt. Express **15**, 17458 (2007).
[5] B.-S. Song, S. Noda, T. Asano, and Y. Akahane, Nature Mater. **4**, 207 (2005).
[6] Y. Takahashi, H. Hagino, Y. Tanaka, B.-S. Song, T. Asano, and S. Noda, Opt. Express **15**, 17206 (2007).
[7] M. Barth, N. Nüsse, J. Stingl, B. Löchel, and O. Benson, Appl. Phys. Lett. **93**, 021112 (2008).
[8] J. S. Foresi, P. R. Villeneuve, J. Ferrera, E. R. Thoen, G. Steinmeyer, S. Fan, J. D. Joannopoulos, L. C. Kimerling, H. I. Smith, and E. P. Ippen, Nature (London) **390**, 143 (1997).
[9] P. B. Deotare, M. W. McCutcheon, I. W. Frank, M. Khan, and M. Lončar, Appl. Phys. Lett. **94**, 121106 (2009).
[10] M. Eichenfield, R. Camacho, J. Chan, K. J. Vahala, and O. Painter, Nature (London) **459**, 550 (2009).
[11] M. W. McCutcheon and M. Lončar, Opt. Express **16**, 19136 (2008).
[12] M. Notomi, E. Kuramochi, and H. Taniyama, Opt. Express **16**, 11095 (2008).
[13] J. Chan, M. Eichenfield, R. Camacho, and O. Painter, Opt. Express **17**, 3802 (2009).
[14] R. D. Kekatpure and M. L. Brongersma, Phys. Rev. A **78**, 023829 (2008).
[15] D. K. Armani, T. J. Kippenberg, S. M. Spillane, and K. J. Vahala, Nature (London) **421**, 925 (2003).
[16] J. Goh, I. Fushman, D. Englund, and J. Vučković, Opt. Express **15**, 8218 (2007).
[17] D. Englund, I. Fushman, and J. Vučković, Opt. Express **13**, 5961 (2005).
[18] J. Lu and J. Vučković, arXiv:0912.4425v1 (unpublished).
[19] H. Altug and J. Vučković, Appl. Phys. Lett. **86**, 111102 (2005).
[20] D. Englund, A. Faraon, I. Fushman, N. Stoltz, P. Petroff, and J. Vučković, Nature (London) **450**, 857 (2007).
[21] L. Pavesi, L. Dal Negro, C. Mazzoleni, G. Franzò, and F. Priolo, Nature (London) **408**, 440 (2000).
[22] K. Rivoire, A. Kinkhabwala, F. Hatami, W. T. Masselink, Y. Avlasevich, K. Muellen, W. E. Moerner, and J. Vučković, Appl. Phys. Lett. **95**, 123113 (2009).